



Improving high-temperature energy storage performance of PI dielectric capacitor films through boron nitride interlayer

Kaiyi Zhang¹ · Zhuyu Ma¹ · Hua Deng¹ · Qiang Fu¹

Received: 26 July 2021 / Revised: 9 August 2021 / Accepted: 13 August 2021 / Published online: 23 August 2021
© The Author(s), under exclusive licence to Springer Nature Switzerland AG 2021

Abstract

As an important power storage device, the demand for capacitors for high-temperature applications has gradually increased in recent years. However, drastically degraded energy storage performance due to the critical conduction loss severely restricted the utility of dielectric polymers at high temperatures. Hence, we propose a facile preparation method to suppress the conductivity loss of polyimide (PI) films by inserting boron nitride interlayer. The experimental results and computational simulations indicate that consecutive boron nitride interlayer has better effect on suppressing leakage current density of the entire material compared with uniform dispersed boron nitride nanosheet (BNNS) composite films. The experimental results show that the leakage current density of PI films is reduced by an order of magnitude and a classy energy density of 2.58 J/cm³ at a charge–discharge efficiency of 90% has been achieved at 150 °C, far better than pristine PI (0.75 J/cm³ of energy density and 65% of efficiency under 275 kV/mm and at 150 °C). The method we reported in this work is applicable to a variety of polymer dielectric films produced by solution casting for elevated temperature energy storage application.

Keywords High-temperature energy storage · PI · Boron nitride interlayer · Leakage current density

1 Introduction

Electrostatic capacitors possess the ultra-high power density and fast charge–discharge rate that electrochemical capacitors and batteries cannot match, which enable them to have broad application prospects in modern electrical and electronic systems, such as hybrid electric vehicles (HEVs), grid-connected photovoltaic systems, wind power generation, and underground oil and gas exploration [1–3]. However, high temperature, high current, and high power are the working conditions faced by capacitors in actual application scenarios [4, 5]. For example, the operating temperature of capacitors in HEVs is 140 °C, and even higher than 250 °C in underground oil and gas exploration. However, the current state-of-the-art polymer-based dielectric biaxially oriented polypropylene (BOPP) has a maximum operating temperature of no more than 105 °C [6], which requires an additional cooling system to ensure the effective operation

of BOPP, resulting in reduced energy efficiency and higher cost and weight [7]. Therefore, there are urgent needs to develop polymer dielectric films that can adapt to extreme environments.

To realize stable application of capacitors at high temperatures, it is inevitable to select polymers with high glass transition temperature (T_g). At present, the polymer dielectric materials with high T_g include polyimide (PI, $T_g \approx 360$ °C), polyetherimide (PEI, $T_g \approx 217$ °C), polyetheretherketone (PEEK, $T_g \approx 143$ °C), polycarbonate (PC, $T_g \approx 150$ °C), fluoropolyester (FPE, $T_g \approx 330$ °C), and polyamide-imide (PAI, $T_g > 300$ °C) [8]. Although the T_g of these polymers are relatively high, their energy density and efficiency deteriorate seriously contrast with that at room temperature (RT) due to rapidly increased conduction loss. For instance, at 150 °C and 250 MV/m, the energy density and efficiency of PEEK is 0.5 J/cm³ and 30%. This is because the barrier height at the interface between electrode and dielectric material is reduced due to the dual effects of high temperature and mirror force, so that electrons are more easily injected from electrode [9, 10]. In addition, most of the molecular chain structures of high-temperature resistant polymers have a large number of benzene rings, resulting in a lower band gap [11–13] (PEI of 3.2 eV contrast with PP of 8.8 eV), which makes electrons easier to

✉ Hua Deng
huadeng@scu.edu.cn

¹ College of Polymer Science and Engineering, State Key Laboratory of Polymer Materials Engineering, Sichuan University, Chengdu 610065, People's Republic of China

excite and aggravates the increase in leakage current [14]. Moreover, the Joule heating effect caused by the conduction loss accelerates the breakdown process under high temperature and high electric field, which seriously affects the long-term stability of polymer dielectric.

Recent years, researchers have proposed some methods to suppress leakage current. For instance, Wang found that fillers with wide band gap have obvious impact on energy storage performance and E_b of dielectric nanocomposites [15, 16]. Li utilized the strong electrostatic attraction of molecular semiconductors to immobilize free electrons and impede electric charge injection and transport in dielectric polymers [17]. In addition, inorganic materials of wide band gap such as silicon dioxide (SiO_2) and boron nitride have been deposited on dielectric films via chemical vapor deposition (CVD) to increase the height of electrode/dielectric interface barrier [18, 19]. Thereby, the injection of electrons is suppressed. However, large-scale production through either uniformly dispersed fillers or CVD is an unsolved problem at present. Therefore, there is an urgent need for a scalable method to improve the energy storage performance of polymer dielectric materials at elevated temperature.

BNNS with wide band gap of 5.9 eV has been shown to have significant effect on improving E_b and charge–discharge efficiency of polymer-based dielectric nanocomposites owing to its high intrinsic E_b and insulation [20–28]. These advantages make it an ideal carrier scattering center. PI is a very common high-temperature resistant polymer material, and its precursor PAA has good solubility which means it has excellent film-forming properties. Mature preparation process and low price make PI have the potential of scalable application in the field of high-temperature dielectric energy storage. However, PI possess poor high-temperature dielectric energy storage performance caused by severe conduction loss. To solve this problem, dielectric films for high-temperature application combined PI and boron nitride interlayer are prepared by typical solution casting which exhibits the advantages of low energy consumption, scalability, and simple preparation process compared with CVD. The experiment results indicate that a small amount of boron nitride interlayer can increase the E_b and suppress leakage current, leading to significant increase in energy storage density at high temperature. Method reported in this paper provides a scalable and effective approach for the preparation of high-temperature polymer dielectric materials.

2 Experiment

2.1 Materials

The commercially available polyamic acid (PAA) solution was supplied by RTP (USA). N, N-dimethylacetamide

(DMAc, water ≤ 30 ppm (by K.F.), 99.8%, Safe-Dry with molecular sieve) was purchased from Adamas. Hexagonal boron nitride (h-BN) powders (2–3 μm , > 99%) were purchased from Qinhuangdao Eno High-Tech Material Development Co., Ltd (China). Isopropanol (IPA, 99.8%) was purchased from Adamas. All above materials are used directly without further purification.

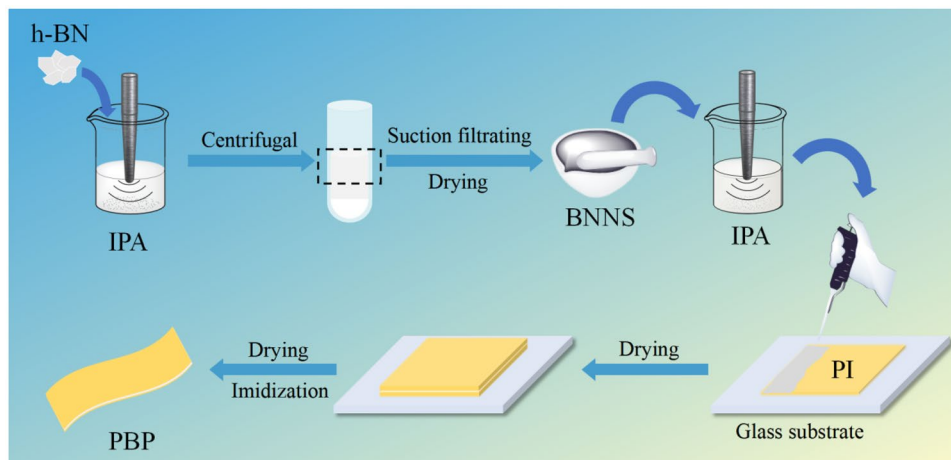
2.2 Preparation of BNNS

BNNS were fabricated via liquid-phase exfoliation method. A total of 3 g h-BN powders were dispersed in 100 ml IPA and 100 ml deionized water. After 5 min sonication bath dispersion, the mixture was placed into cell grinder with ice bath for 480 min. The obtained dispersions were centrifuged at 4000 rpm for 20 min and then collected the supernatant. Afterward, BNNS was obtained via filtering and oven drying. Finally, the dried BNNS was grinded for subsequent use.

2.3 Preparation of sandwich structured composite films

The fabrication process of sandwich-structured films is illustrated in Fig. 1. A total of 60 mg BNNS powders were dispersed in 20 ml IPA and then ultrasonic dispersed for 240 min to obtain stable dispersions. Then, PAA solution with a certain mass fraction was casted onto a clean glass substrate through a doctor blade served as the first layer. The glass substrates were placed into vacuum oven for 1 day to remove solvent. After the first layer of PAA was dry, BNNS dispersions were casted onto PAA film repeatedly in the same way and dried thoroughly and the solid content and dispersions volume of BNNS can be precisely controlled by pipetting gun. To be specific, using a pipette to suck up 250 μL of boron nitride dispersions, adjusting the height of the doctor blade so that the boron nitride dispersions can just cover the entire PPA base film, putting it in a 70 °C blast oven for 5 min to dry, and then taking it out and carry out the above operations until the total volume of the scraping dispersions is the desired total volume. Last, the composites films were put into vacuum oven and further imidized. The curing conditions are 100 °C, 150 °C, 200 °C, 230 °C, and 260 °C for 1 h each. Afterwards, composite films were peeled off and dried for 1 day. Six sandwich structure films were donated as PBP2.25, PBP4.5, PBP6.75, PBP9, PBP11.25, and PBP13.5, and the number represented the mass of boron nitride interlayer (the unit of mass is milligram). The thickness of PBP films is 10–15 μm .

Fig. 1 Schematic diagram of PBP films preparation process



2.4 Characterization

The morphology of PI and PBP films were characterized with scanning electron microscopy (SEM, JEOL JSM5900LV), and the surface morphology and thickness of exfoliated BNNS was measured by atomic force microscope (AFM). X-ray diffraction (XRD, X'Pert pro MPD, Philips Company) was used to characterize the h-BN crystal structure before and after exfoliation with scanning range of 10–90°. Fourier transform infrared spectroscopy (FT-IR) was used to characterize the chemical structure of PI and PBP films. The dielectric constant and dielectric loss were measured by Novocontrol concept 50 in the frequency range of 1–10⁶ Hz at RT, 80 °C, 150 °C, and 200 °C. The breakdown strength (E_b) of the PBP were measured by breakdown voltage tester (SG-255G, DC voltage) with test voltage range of 0–20 kV and test temperature of RT, 80 °C and 150 °C. Hysteresis loop tester (Premier II-100 V, American Radiant Company) was used to characterize polarization of materials under alternating electric field and different test temperature. Differential scanning calorimeter (DSC, PerkinElmer Instruments) is used to confirm the PI curing is complete under a nitrogen atmosphere and at a heating/cooling rate of 10 °C min⁻¹. TGA was conducted on a thermogravimetric analyzer (TG 209F1 Iris, Netzsch, Germany) under dry air.

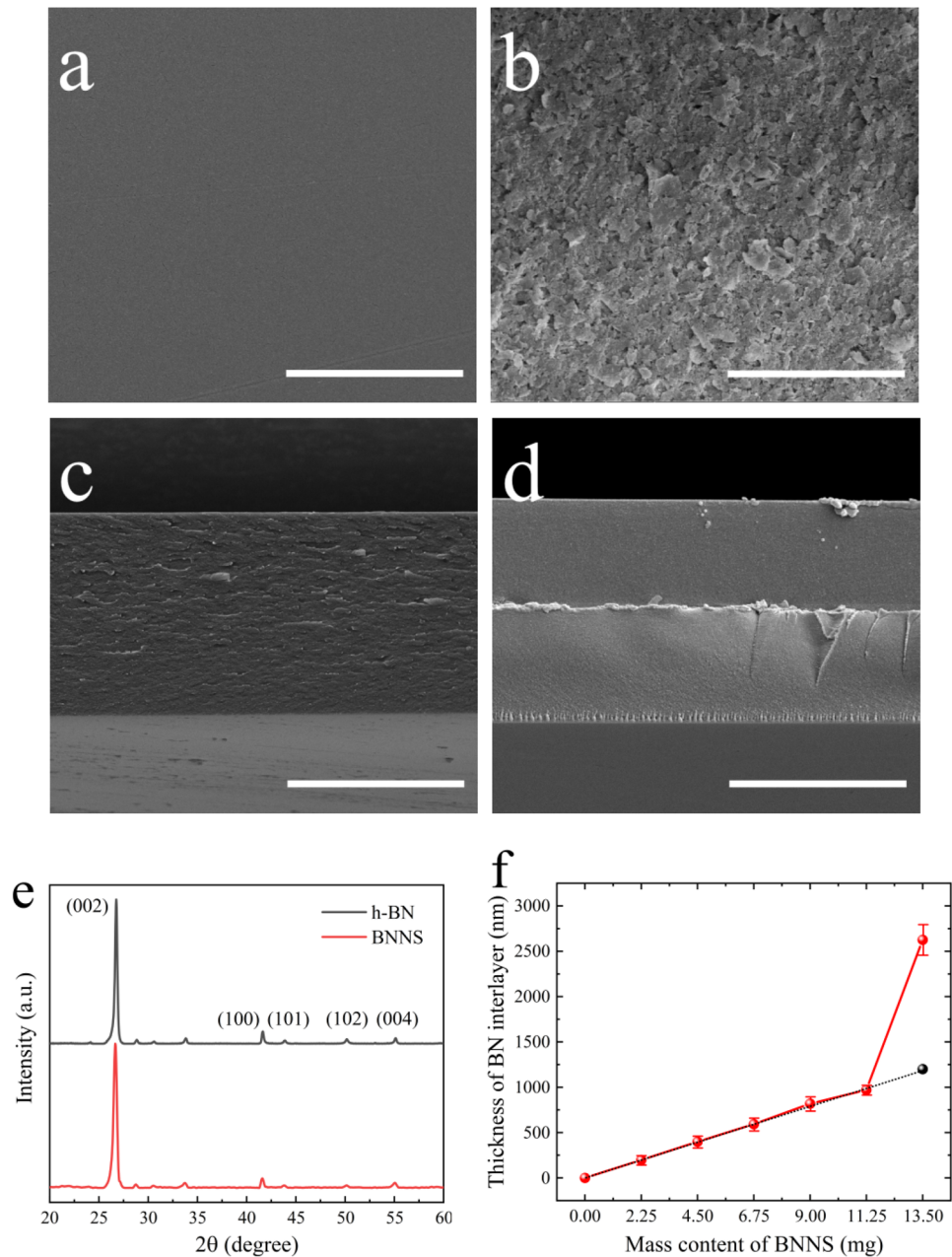
3 Results and discussion

The morphology of BNNS after exfoliation is examined using AFM as shown in Fig. S1. BNNS exposes obvious difference in diameter and its thickness is about 20 nm, which indicate BNNS was successfully exfoliated. Although the diameter of BNNS was in the relatively large range of 100–500 nm, the smaller BNNS can embed between the large BNNS to make boron nitride interlayer more compact. As show in Figs. 2b and S2a–e, it is noted that BNNS

were forced to arrange in parallel by shearing effect of doctor blade and overlap with each other. Different from integral and dense boron nitride film fabricated via CVD, boron nitride interlayer of different mass content shows rough and porous morphology compared to smooth and flat PI surface. This distinguishing feature may help the upper and lower layers of PI film bond well since PAA can be connected through holes. To verify whether the crystal structure of h-BN has changed after ultrasonic exfoliation, XRD was carried out, and the result is shown in Fig. 2e, it can be observed that the distinctive peak of BNNS was located at 26.7° the same as h-BN, which suggest the crystal structure is well preserved even though going through 480-min ultrasound exfoliation. Boron nitride interlayer was fabricated via solution casting and drying which means that good uniformity and stability of BNNS dispersions in IPA are important to the quality of boron nitride interlayer. Otherwise, the boron nitride interlayer deposited by volatilizing solvent is likely to form visible unevenness and granular agglomerates. Therefore, BNNS dispersion was free settled for a week and its optical image is shown in Fig. S3. It can be seen that there is no obvious difference compared with the BNNS dispersions just after ultrasonic treatment indicating rather good stability.

The PBP films were fabricated by three individual solution casting process, in order to confirm whether the sandwich structure is formed; the cross-section of PBP films were characterized with SEM as shown in Figs. 2c–d and S2f–j. Each PBP films expose a clear three-layer structure and boron nitride interlayer is located at the middle of PBP and the thickness statistic chart of PBP films is shown in Fig. 2f. It can be confirmed that the thickness of boron nitride interlayer increases linearly with increasing mass content of BNNS at low contents, whereas the thickness of boron nitride interlayer of PBP13.5 is nearly 2.5 μm, far beyond the expected value of 1.2 μm (extrapolated value calculated from the curve, as shown in Fig. 2f). The reasons

Fig. 2 **a–b** SEM images of surface of PI, PBP2.25, respectively. **c–d** Cross-section SEM images of PI, PBP2.25, respectively (all scale bars are 10 μm). **e** Statistical chart of BN interlayer thickness. **f** XRD results for h-BN and BNNS



may be that different from in situ synthesis of inorganic films by CVD and other methods, boron nitride interlayer is deposited on PAA films by solution volatilization, which means that there must be voids between BNNS. With the increase of boron nitride content, the void volume will increase and undesirable accumulation will occur along the vertical direction; this makes the thickness of boron nitride interlayer significantly different at high content. Owing to the good fluidity of PAA solution, when the third layer of PAA covers the boron nitride interlayer, PAA penetrated into voids, causing the greatly increase of thickness of the boron nitride interlayer. The conjecture is further confirmed by Fig. S4. It is observed that compared to the rather flat

surface of PBP2.25, PBP13.5 possess rougher and more porous surface which can be seen at the locations indicated by the marks.

Incomplete curing would greatly reduce the E_b and meanwhile increasing the dielectric loss. To verify that PI based films is fully cured, DSC was performed on the cured PI and the result is shown in Fig. S5a. It is confirmed that the curing conditions used are sufficient for PI to cure completely. Further evidence is shown in Fig. S5b, the absorption band at 3252 cm^{-1} and 1640 cm^{-1} result from the N–H and C=O stretching of PAA and their disappearance indicates that PAA is completely reacted. As shown in Fig. S5c, peaks at 1775 cm^{-1} , 1720 cm^{-1} , 1341 cm^{-1} , and 723 cm^{-1} represent

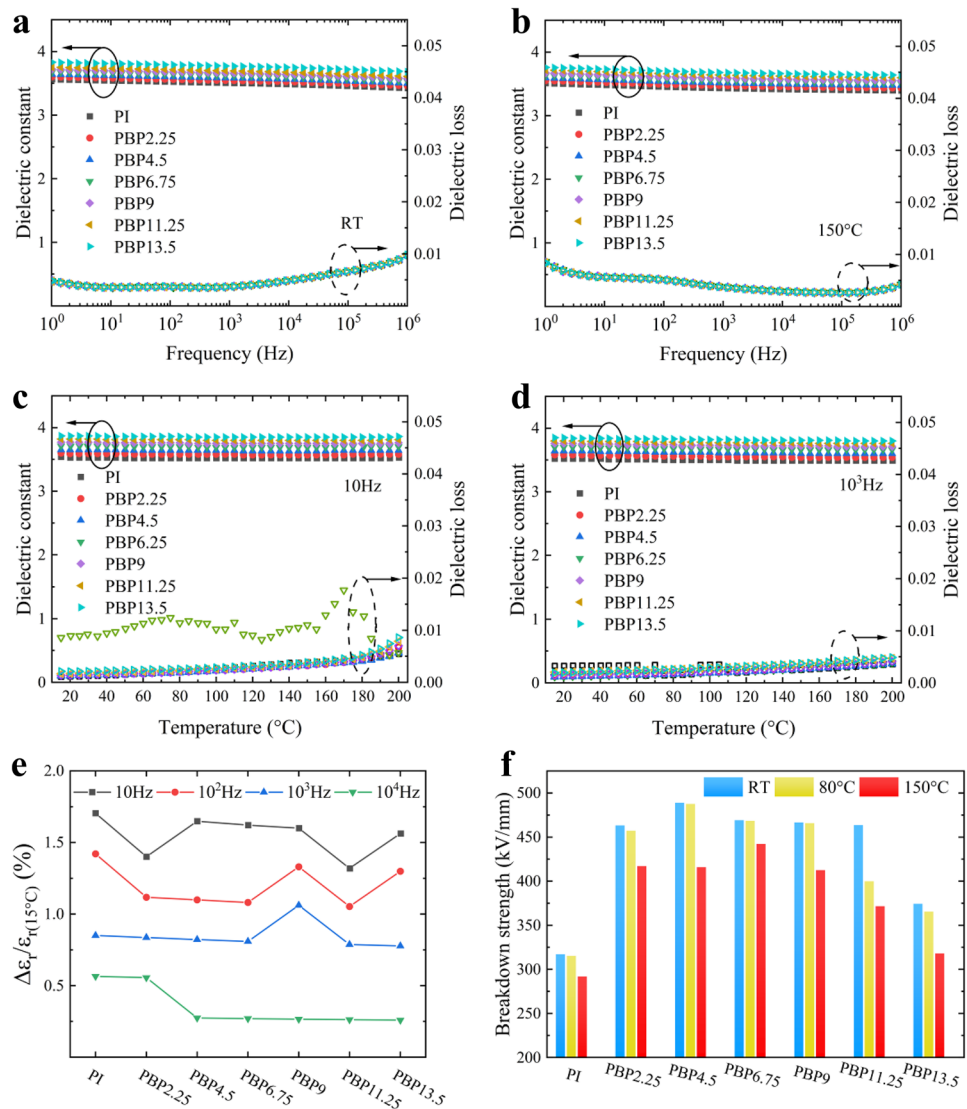
the C=O asymmetric stretching, C=O symmetric stretching, C=N stretching, and C=O bending of PI. The results of FT-IR indicate that PI and PBP films are cured completely.

To reveal the influence of boron nitride interlayer on dielectric performance of PI, the dielectric constant and loss as a function of frequency and temperature were studied. As shown in Figs. 3a–b and S6a, b, PBP films exhibit a slight increase in dielectric constant compared with pristine PI film (from 3.5 to 3.8), attributable to similar dielectric constant of PI ($\epsilon_r = 3.5$) and BNNS ($\epsilon_r \approx 4$). In addition, interfacial polarization caused by the interface between PI and boron nitride interlayer can also cause an increase in dielectric constant [29–36]. Unlike ceramics and conductive fillers, BNNS does not significantly increase the dielectric loss of the composite films due to its intrinsic electrical inertness. As a result, the dielectric loss of each PBP films is under 0.01. The dielectric stability of dielectric films at different temperatures is of great significance for practical

applications, owing to the actual working environment temperature may be variable. In order to verify the temperature stability of dielectric properties of PBP films, continuous tests from 15 to 200 °C were conducted. As shown in Figs. 3c–d and S6c, d, the dielectric constant of PI and PBP films shows independent characteristic with temperature and the variation of dielectric constant is no more than 1.75% at 10 Hz, 10^2 Hz, 10^3 Hz, and 10^4 Hz as shown in Fig. 3e. The variation of dielectric constant of films shows a downward trend as frequency rises. According to the polarization mechanism, several polarizations such as orientational and interface become relaxed as frequency rises which mean they no longer contribute to the increase of dielectric constant [29, 37]. Actually, these two polarizations have a strong dependence on temperature which could lead to the variation in dielectric constant at different temperatures.

The dielectric constant can only reflect the polarization of dielectric materials, but the E_b can determine the maximum

Fig. 3 a–b Dielectric constant and loss of PI, PBP films in the frequency range of 1 to 10^6 Hz. c–d dielectric constant and loss of PI, PBP films in the temperature range of 15 to 200 °C. e The variation in dielectric constant at 15 and 200 °C. f The E_b of PI and PBP films at RT, 80 °C and 150 °C



electric field that materials can load [38]. Without considering energy loss, the greater electric field that materials can load, the greater energy density would be. Therefore, the E_b of PI and PBP films were characterized base on the two-parameter Weibull distribution, which can be described as followed equation:

$$P(E) = 1 - \exp\left[-\left(\frac{E}{E_b}\right)^\beta\right] \quad (1)$$

where $P(E)$ is the cumulative probability of electric failure, E is experimental breakdown strength, E_b is the characteristic breakdown strength of cumulative failure probability of 63.2%, and β is the shape parameter which represent the dielectric reliability of materials. The E_b of PI and PBP films is summarized in Fig. 3f. Apparently, the E_b of PBP films greatly increases with the mass content of BNNS from 2.25 mg to 11.25 mg and further addition of BNNS lead to substantial reduction in improvement of E_b . At RT, the highest E_b of 489 kV/mm is achieved with BNNS mass content of 4.5 mg which is 54.2% higher than pristine PI ($E_b = 317$ kV/mm), and even at the highest mass content of 13.5 mg, the E_b is also increased by 18% compared with PI. Noteworthiness, as shown in Fig. S7, the β value of PBP films is lower than pristine PI, representing the dielectric properties of PI films are more reliable than PBP films. Similarly, the β and E_b of PI and PBP films show the same trend at 80 °C. The reason is supposed to be the macroscopic heterogeneity of boron nitride interlayer. At elevated temperature of 150 °C, the β value of PI decreases from 18.7 to 12.3, suggesting high-temperature condition does have negative impact on the properties of PI films. In contrast, there was no significant decrease in β value of PBP films which proves that boron nitride interlayer has an inhibitory effect on the growth of breakdown phase [39–41]. It is worth noted that the E_b of PBP films show a significant improvement comparing with PI even it has detectable decrease at high temperature. The peak value of 442.3 kV/mm achieves at the BNNS mass content of 6.75 mg, 51% improvement compared to PI. Regardless of the temperature, the E_b of PBP13.5 shows a relatively low enhancement effect. This is due to the high intrinsic E_b of boron nitride, which inhibits the growth of the breakdown phase and improves the E_b . However, when the boron nitride content is high, cavities are easily generated in the boron nitride interlayer. The increase of this kind of defect may make the upper layer PAA solution unable to fully infiltrate when the boron nitride interlayer is very thick which leads to reduction of the E_b . Under the dual effects of these two effects on the increase and decrease of the E_b , the increase of the E_b of PBP13.5 is not very obvious compared with other PBPs.

The actual working conditions of capacitor films generally are alternating high voltage. However, the dielectric

constant and loss can reveal the polarization of dielectric materials, but cannot truly reflect the energy storage performance of dielectric films at high temperatures, because the test voltage applied is only 1 to 2 V. Thus, to further uncover the energy storage performance of PI and PBP films, D-E loops were studied. As shown in Fig. S8, a narrow enclosing area of loop indicates the low energy loss and high D_{\max} suggesting high energy storage density. Owing to the intrinsic linear dielectric properties of PI and BNNS, as shown in Figs. 4a and S9, it is obviously found that the PI and PBP films expose more than 90% efficiency at the electric field up to 475 kV/mm at RT. Due to the enhancement in E_b caused by boron nitride interlayer, PBP11.25 can reach 3.69 J/cm³ at 450 kV/mm comparing with the pristine PI of 1.55 J/cm³ at 300 kV/mm. When temperature rises to 80 °C, as shown in Fig. S10, the D-E loops of PI film become larger with increasing electric field which means conduction loss becomes obvious gradually. The efficiency of PBP films maintain excellent level even at 375 kV/mm shown in Fig. 4b. Among PBPs, PBP2.25 films deliver the energy density of 3.36 J/cm³ and 93% efficiency versus 0.92 J/cm³ and 79% of pristine PI.

In the absence of external cooling system, high-temperature dielectric films are required to have stable energy storage performance at above 140 °C. In order to meet this requirement, D-E loop of PI and PBP films at 150 °C and 200 °C were studied and shown in Figs. S11 and S12. By integrating the curve in Fig. S11, it is found that the conduction loss of PI film increases rapidly with increasing electric field, which indicates that the number of free electrons injected by the electrode and self-excited inside materials increases sharply under high temperature and high electric field. Surprisingly, PBP9 films can still maintain the efficiency of 90% at 375 kV/mm as shown in Fig. 4c, suggesting the boron nitride interlayer does play the role of electron scattering center and barrier. Overall, the improving effect of boron nitride interlayer on energy storage performance is most remarkable at the intermediate mass content and the reasons should be the thickness and compactness of boron nitride interlayer. At low mass content, owing to the pores, the boron nitride interlayer is not thick enough to completely block the electrons accelerated by electric field and partial electrons can still pass through the boron nitride interlayer by pores. At high mass content, the number of electrons conducted along the interface increases due to increased number of defects. In spite of the possibilities mentioned above, compared with PI films, PBP films still exhibit obvious effect of restraining conduction loss, which is attributed to the intrinsic characteristics of wide band gap and high insulation of BNNS. As a result, PBP9 possess an energy density of 2.58 J/cm³ and efficiency of 90%, much higher than pristine PI of 0.75 J/cm³ and 65% at

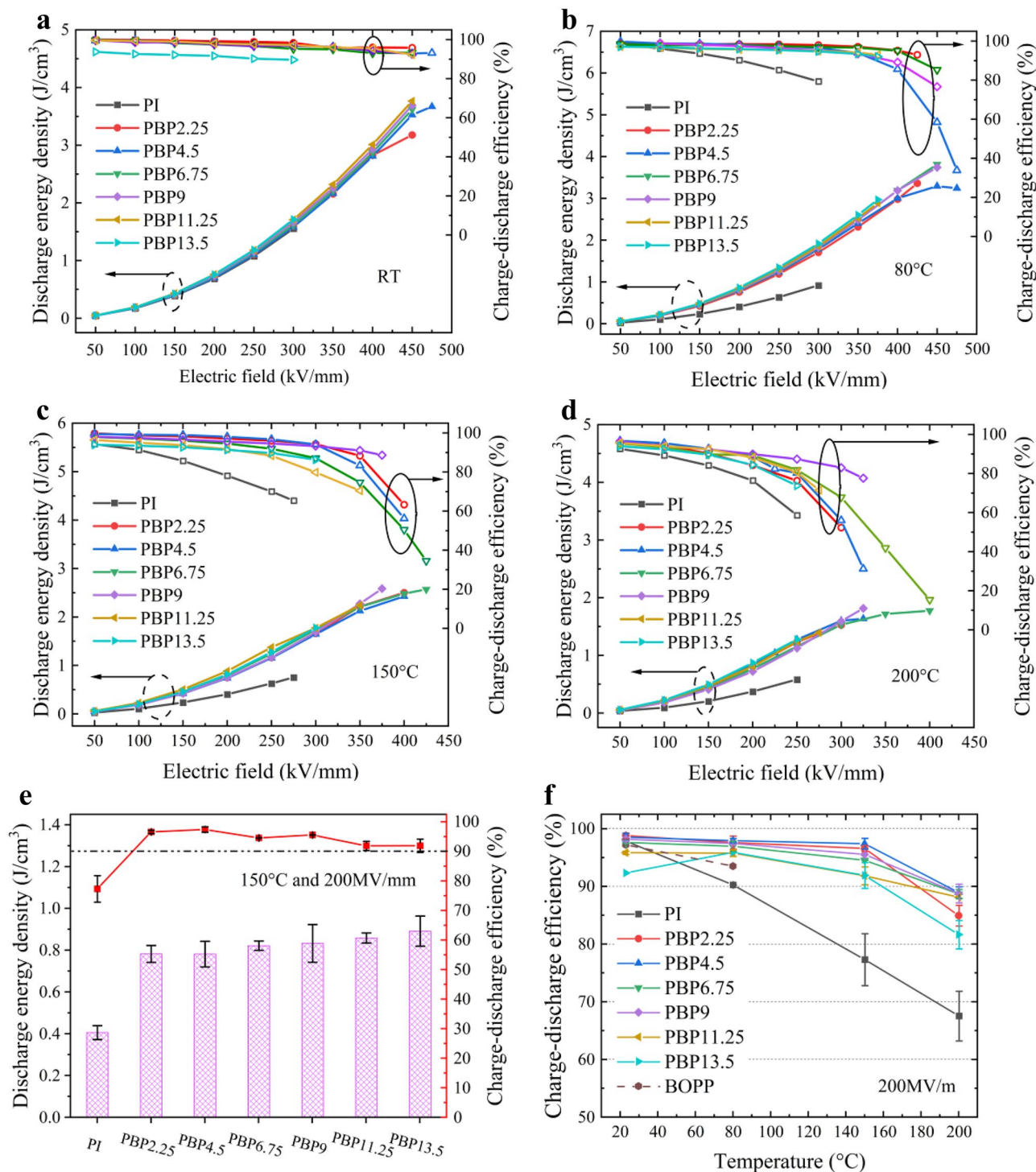


Fig. 4 a–d Discharge energy density and efficiency of PI and PBP films at RT, 80 °C, 150 °C, and 200 °C. e Discharge energy density and charge–discharge efficiency of PI and PBP at 150 °C and 200

MV/mm. f At the electric field of 200 MV/m, the charge–discharge efficiency of PI, BOPP, and PBP at RT, 80 °C, 150 °C, and 200 °C

150 °C. At high temperature, the E_b of dielectric materials is also a considerable factor that restricts the increase in energy storage density, because the E_b directly determines the maximum loaded alternating electric field of

dielectric materials, which in turn affects the maximum electric displacement. PBP films exhibit higher E_b than pristine PI because of the impediment to the growth of breakdown phase of boron nitride interlayer.

PI possess excellent high-temperature resistance performance. According to the type of monomer diamine, PI synthesized by aromatic diamine has a decomposition temperature of near 600 °C which means PI has the possibility of application at higher temperatures [42, 43]. According to the TGA result shown in Fig. S13, the decomposition temperature of PI and PBP films is around 585 °C, suggesting excellent thermal stability. As shown in Fig. 4d, obviously, energy storage properties decline sharply at 200 °C. However, the PBP9 films can maintain at around 80% efficiency and 1.81 J/cm³ versus PI of 0.58 J/cm³ and 58%. In order to explore the performances of PI and PBP films in practical application scenarios, the working conditions of capacitors in hybrid electric vehicles of 150 °C and 200 kV/mm were chosen for comparison. As shown in Fig. 4e, all PBP films have an efficiency of over 90% and the energy density of PBP films is twice as much as PI films. Figure 4f compares the charge–discharge efficiency of PI films, PBP films and BOPP as a function of temperature measured at 200 MV/m. Obviously, the PBP films exhibit better dielectric properties than PI and BOPP. At 150 °C, PBP films have a charge–discharge efficiency of over 90%. Even at 200 °C, PBP films still maintain an efficiency of over 80% while that of PI films drop to below 70%.

Since the polarization of PBP films has not been significantly improved, the enhancement in high-temperature energy storage performance of materials is mainly due to the improvement in charge–discharge efficiency and the main reasons for the reduction of efficiency of materials is determined by conduction loss. The conduction loss is reflected in the form of leakage current density. Thus, in order to further illustrate the restraining effect of boron nitride interlayer on leakage current, leakage current density was characterized

and the results at 150 °C are shown in Fig. 5a. While the leakage current density increases with electric field, the value of leakage current density of PBP films is consistently lower than that of PI and the difference reaches the maximum at 200 kV/mm. Summarizing the leakage current density of PI and PBP films at 200 kV/mm in a chart (Fig. 5b), it is obvious that the leakage current density of PBP films achieves a substantial reduction contrast with pristine PI. The lowest leakage current density of 2.16×10^{-8} A/cm² is achieved at BNNS mass content of 9 mg, nearly 1/35 of PI, and even the PBP13.5 shows leakage current density 1/7 of PI. These results prove that boron nitride interlayer has clear effect on restraining leakage current.

To further demonstrate the superiority of the boron nitride interlayer over traditional polymer composites on restraining leakage current, finite element simulation of PBP and randomly parallel distributed PI/BNNS composite were conducted by COMSOL. The models are shown in Fig. 6a, and the simulation results are shown in Fig. 6b–c. In PBP, it can be seen that the current density in most of the regions are at relatively low level contrast with PI/BNNS of almost half of the regions are at a rather high level. Interestingly, as shown in Fig. S14, the current density of upper surface of PBP shows much lower than PI/BNNS composite; this may indicate that the number of electrons injected into the upper surface is less than that of PI/BNNS. In addition, it is obvious that high current density areas are blocked by the boron nitride interlayer, while the high current density region connects the upper and lower surfaces in the PI/BNNS model. This suggests that the boron nitride interlayer acts as an effective electron scattering center and barrier to hinder the transportation of free electrons, and leading to enhancement in energy storage efficiency.

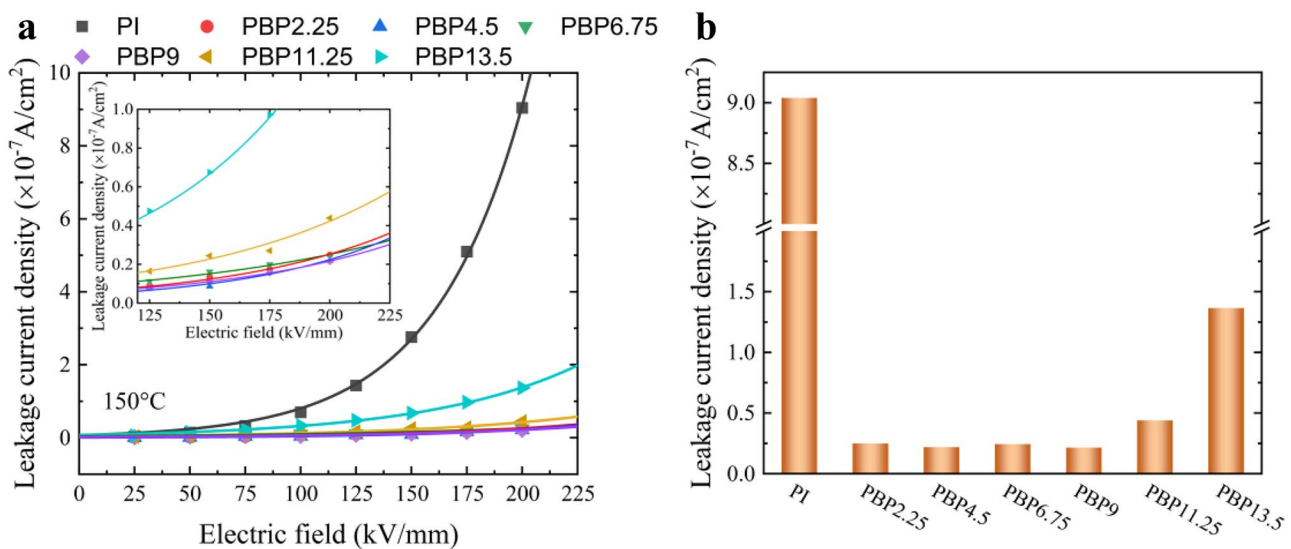
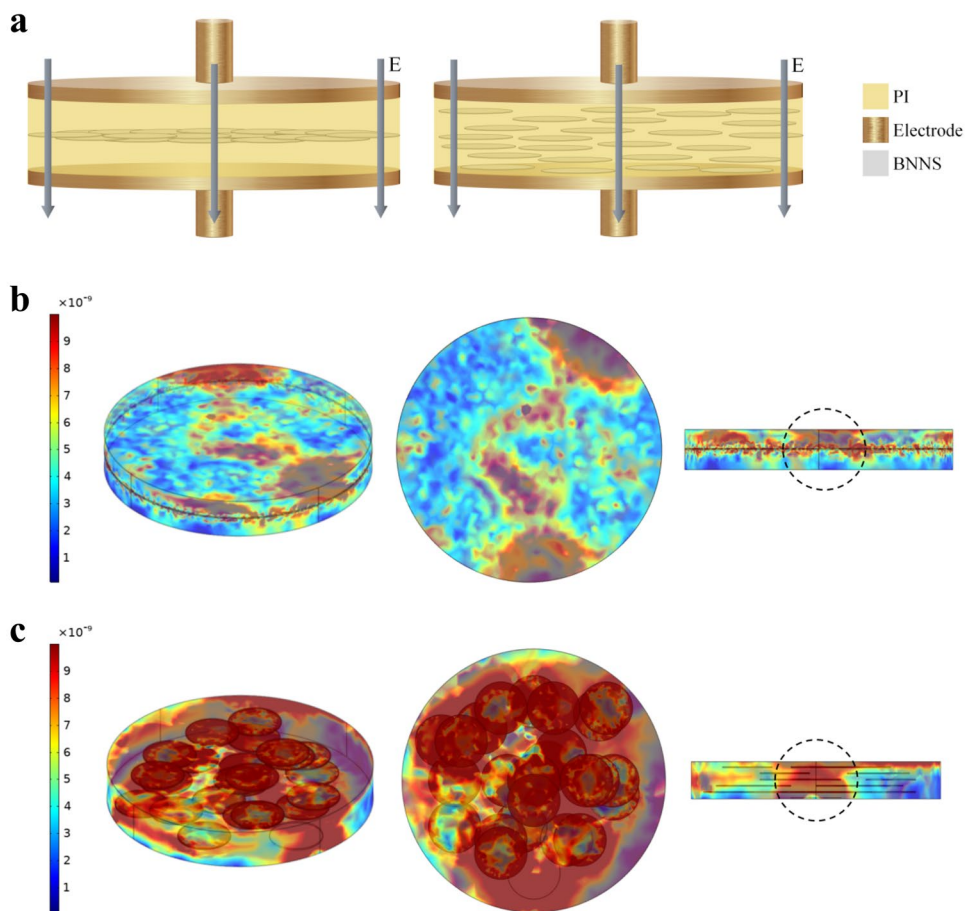


Fig. 5 a Leakage current density of PI and PBP films at 150 °C. b Leakage current density of PI and PBP films at 150 °C and 200 kV/mm

Fig. 6 a Schematic diagram of computational simulation models of PBP films (left) and randomly parallel distributed PI/BNNS composite films (right). **b–c** Simulation results of three-dimensional current density (A/m^2) distribution of above two models (from left to right are XYZ-view, XY-view, XZ-view). Loading electric field is 200 kV/mm and lower surface grounding



In order to figure out the advantage of boron nitride interlayer, Fig. 7 lists the energy storage performances of dielectric polymer composites at 150 °C and 200 °C in

recent years [44–52]. It can be seen that PBP films in this work show classy energy storage performance than most of the high-temperature polymer composites reported recently.

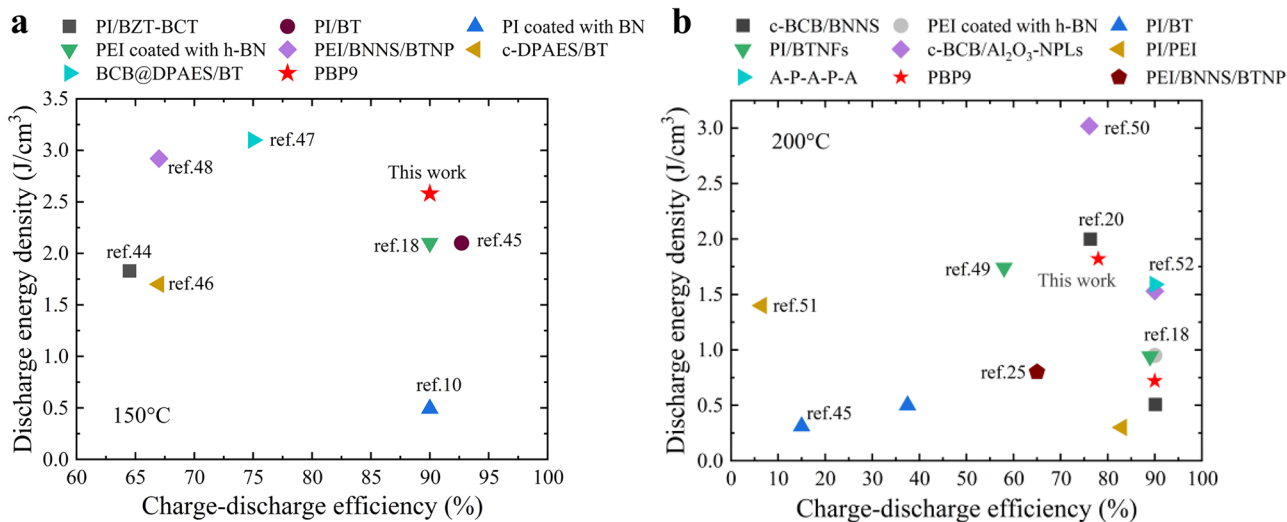


Fig. 7 Comparison charts of discharge energy density and charge-discharge efficiency of dielectric materials at **a** 150 °C and **b** 200 °C. BZT-BCT: $0.5Ba(Zr_{0.2}Ti_{0.8})O_3-0.5(Ba_{0.7}Ca_{0.3})TiO_3$. BN boron nitride, BTNP barium titanate nanoparticles, c-DPAES crosslinked

poly(arylene ether sulfone)s, BT barium titanate, c-BCB crosslinked divinyltetramethyldisiloxanebis(benzocyclobutene), BCB benzocyclobutene, BTNFs barium titanate nanofibers, Al_2O_3 -NPLs alumina nanoplates, A-P-A-P-A Al_2O_3 -PI- Al_2O_3 -PI- Al_2O_3

Especially in Fig. 7a, the energy density at the level of efficiency above 90% (or the maximum value of efficiency available for capacitors), PBP9 can reach 2.58 J/cm^3 which is larger than other PI composites. For example, PI/BaTiO₃, PI/BZT-BCT, and PI/BN (PI coated with BN through physical vapor deposition) have energy density of 2.1 J/cm^3 , 0.493 J/cm^3 , and 1.83 J/cm^3 , respectively. At higher temperature of 200 °C, Fig. 7b summarizes up-to-date works which studied energy storage performance at 200 °C. Although the energy storage performance of PBP9 is not the top at 200 °C, energy density of 1.82 J/cm^3 and efficiency of 78% can also reach the class level among previous works. In addition, the energy storage performance of PBP films was compared with that of high-temperature resistant polymers in literature and the results are shown in Fig. S15. It is obviously found that the energy storage performances of PBP9 outperform PC, PEI, FPE, and PEEK, showing great application potential. Therefore, embedding boron nitride interlayer into polymer matrix is a feasible and effective method.

4 Conclusions

In this work, sandwich structure composite films were prepared by embedding boron nitride interlayer into PI matrix via simple layer-by-layer casting method. The BNNS directly overlap with each other on PI surface, forming a compact layer of boron nitride located at the middle of PI film. Compared with the traditional solution mixing and casting, the method used in this work can achieve obvious improvement in energy storage performance with rather low loadings of BNNS. It was experimentally confirmed that the boron nitride interlayer serves as an electron scattering center and barrier that suppress the leakage current and hinder the propagation of breakdown phase. Such result was further confirmed by computational simulation. Consequently, the E_b and charge–discharge efficiency were significantly improved due to the boron nitride interlayer. As a result, E_b of PBP9 (442.3 kV/mm) exhibit 41% higher than pristine PI at 150 °C and greatly improved energy storage density of 2.58 J/cm^3 versus 0.75 J/cm^3 of PI. This work provides a feasible and scalable strategy for designing high performance dielectric polymer composites used at elevated temperatures.

Supplementary information The online version contains supplementary material available at <https://doi.org/10.1007/s42114-021-00329-7>.

Funding This work was supported by the National Natural Science Foundation of China (51922071).

Declarations

Conflict of interest The authors declare no competing interests.

References

- Li Q, Yao FZ, Liu Y, Zhang G, Wang H, Wang Q (2018) High-temperature dielectric materials for electrical energy storage. *Annu Rev Mater Res* 48(1):219–243. <https://doi.org/10.1146/annurev-matsci-070317-124435>
- Ru J, Min D, Lanagan M, Li S, Chen G (2021) Enhanced energy storage properties of thermostable sandwich-structured BaTiO₃/polyimide nanocomposites with better controlled interfaces. *Mater Des* 197. <https://doi.org/10.1016/j.matdes.2020.109270>
- Fan M, Hu P, Dan Z, Jiang J, Sun B, Shen Y (2020) Significantly increased energy density and discharge efficiency at high temperature in polyetherimide nanocomposites by a small amount of Al₂O₃ nanoparticles. *J Mater Chem A* 8(46):24536–24542. <https://doi.org/10.1039/d0ta08908g>
- Zhou Y, Wang Q (2020) Advanced polymer dielectrics for high temperature capacitive energy storage. *J Appl Phys* 127(24). <https://doi.org/10.1063/5.0009650>
- Tan DQ (2020) The search for enhanced dielectric strength of polymer-based dielectrics: a focused review on polymer nanocomposites. *J Appl Polym Sci* 137(33). <https://doi.org/10.1002/app.49379>
- Tan DQ (2019) Review of polymer-based nanodielectric exploration and film scale-up for advanced capacitors. *Adv Func Mater* 30(18). <https://doi.org/10.1002/adfm.201808567>
- Li Y, Cheng S, Wang S, Yuan C, Luo Z, Zhu Y et al (2021) Multilayered ferroelectric polymer composites with high energy density at elevated temperature. *Compos Sci Technol* 202. <https://doi.org/10.1002/10.1016/j.compscitech.2020.108594>
- Wang Y, Li Z, Wu C, Cao Y (2020) High-temperature dielectric polymer nanocomposites with interposed montmorillonite nanosheets. *Chem Eng J* 401. <https://doi.org/10.1016/j.cej.2020.126093>
- Chiu FC (2014) A review on conduction mechanisms in dielectric films. *Adv Mater Sci Eng* 2014:1–18. <https://doi.org/10.1155/2014/578168>
- Cheng S, Zhou Y, Hu J, He J, Li Q (2020) Polyimide films coated by magnetron sputtered boron nitride for high-temperature capacitor dielectrics. *IEEE Trans Dielectr Electr Insul* 27(2):498–503. <https://doi.org/10.1109/TDEI.2020.008592>
- Zhu L (2014) Exploring strategies for high dielectric constant and low loss polymer dielectrics. *J Phys Chem Lett* 5(21):3677–3687. <https://doi.org/10.1021/jz501831q>
- Wu C, Deshmukh AA, Li Z, Chen L, Alamri A, Wang Y et al (2020) Flexible temperature-invariant polymer dielectrics with large bandgap. *Adv Mater* 32(21). <https://doi.org/10.1002/adma.202000499>
- Wen F, Zhang L, Wang P, Li L, Chen J, Chen C et al (2020) A high-temperature dielectric polymer poly(acrylonitrile butadiene styrene) with enhanced energy density and efficiency due to a cyano group. *J Mater Chem A* 8(30):15122–15129. <https://doi.org/10.1039/d0ta03540h>
- Bao Z, Hou C, Shen Z, Sun H, Zhang G, Luo Z et al (2020) Negatively charged nanosheets significantly enhance the energy-storage capability of polymer-based nanocomposites. *Adv Mater* 32(25). <https://doi.org/10.1002/adma.201907227>
- Ai D, Li H, Zhou Y, Ren L, Han Z, Yao B et al (2020) Tuning nanofillers in in situ prepared polyimide nanocomposites for high-temperature capacitive energy storage. *Adv Energy Mater* 10(16). <https://doi.org/10.1002/aenm.201903881>
- Ren L, Yang L, Zhang S, Li H, Zhou Y, Ai D et al (2021) Largely enhanced dielectric properties of polymer composites with HfO₂ nanoparticles for high-temperature film capacitors. *Compos Sci Technol* 201. <https://doi.org/10.1016/j.compscitech.2020.108528>
- Yuan C, Zhou Y, Zhu Y, Liang J, Wang S, Peng S et al (2020) Polymer/molecular semiconductor all-organic composites

- for high-temperature dielectric energy storage. *Nat Commun* 11(1):3919. <https://doi.org/10.1016/10.1038/s41467-020-17760-x>
18. Azizi A, Gadinski MR, Li Q, AlSaud MA, Wang J, Wang Y et al (2017) High-performance polymers sandwiched with chemical vapor deposited hexagonal boron nitrides as scalable high-temperature dielectric materials. *Adv Mater* 29(35). <https://doi.org/10.1002/adma.201701864>
 19. Zhou Y, Li Q, Dang B, Yang Y, Shao T, Li H et al (2018) A scalable, high-throughput, and environmentally benign approach to polymer dielectrics exhibiting significantly improved capacitive performance at high temperatures. *Adv Mater* 30(49). <https://doi.org/10.1002/adma.201805672>
 20. Li Q, Chen L, Gadinski MR, Zhang S, Zhang G, Li U et al (2015) Flexible high-temperature dielectric materials from polymer nanocomposites. *Nature* 523(7562):576–579. <https://doi.org/10.1038/nature17673>
 21. Wu L, Wu K, Lei C, Liu D, Du R, Chen F et al (2019) Surface modifications of boron nitride nanosheets for poly(vinylidene fluoride) based film capacitors: advantages of edge-hydroxylation. *J Mater Chem A* 7(13):7664–7674. <https://doi.org/10.1039/c9ta00616h>
 22. Liu G, Zhang T, Feng Y, Zhang Y, Zhang C, Zhang Y et al (2020) Sandwich-structured polymers with electrospun boron nitride layers as high-temperature energy storage dielectrics. *Chem Eng J* 389. <https://doi.org/10.1016/j.cej.2020.124443>
 23. Wu L, Luo N, Xie Z, Liu Y, Chen F, Fu Q (2020) Improved breakdown strength of Poly(vinylidene Fluoride)-based composites by using all ball-milled hexagonal boron nitride sheets without centrifugation. *Compos Sci Technol* 190. <https://doi.org/10.1016/j.compscitech.2020.108046>
 24. Zhang X, Chen H, Ye H, Liu A, Xu L (2020) Enhanced interfacial polarization in poly(vinylidene fluoride-chlorotrifluoroethylene) nanocomposite with parallel boron nitride nanosheets. *Nanotechnol* 31(16). <https://doi.org/10.1088/1361-6528/ab69b4>
 25. Li H, Ren L, Ai D, Han Z, Liu Y, Yao B et al (2019) Ternary polymer nanocomposites with concurrently enhanced dielectric constant and breakdown strength for high-temperature electrostatic capacitors. *InfoMat* 2(2):389–400. <https://doi.org/10.1002/inf2.12043>
 26. Shi XT, Zhang RH, Ruan KP, Ma TB, Guo YQ, Gu JW (2021) Improvement of thermal conductivities and simulation model for glass fabrics reinforced epoxy laminated composites via introducing hetero-structured BNN-30@BNNS fillers. *J Mater Sci Technol* 82:239–249. <https://doi.org/10.1016/j.jmst.2021.01.018>
 27. Ruan KP, Yan H, Zhang SJ, Shi XT, Guo YQ, Gu JW (2021) In-situ fabrication of hetero-structured fillers to significantly enhance thermal conductivities of silicone rubber composite films. *Compos Sci Technol* 210. <https://doi.org/10.1016/j.compscitech.2021.108799>
 28. Tang L, He MK, Na XY, Guan XF, Zhang RH, Zhang JL, Gu JW (2015) Functionalized glass fibers cloth/spherical BN fillers/epoxy laminated composites with excellent thermal conductivities and electrical insulation properties. *Composites Commun* 16:5–10. <https://doi.org/10.1016/j.coco.2019.08.007>
 29. Sherkar TS, Koster LJ (2015) Dielectric effects at organic/inorganic interfaces in nanostructured devices. *ACS Appl Mater Interfaces* 7(22):11881–11889. <https://doi.org/10.1021/acsami.5b01606>
 30. Zhou Y, Yuan C, Wang S, Zhu Y, Cheng S, Yang X et al (2020) Interface-modulated nanocomposites based on polypropylene for high-temperature energy storage. *Energy Storage Mater* 28:255–263. <https://doi.org/10.1016/j.ensm.2020.03.017>
 31. Ji W, Deng H, Sun C, Fu Q (2019) Nickel hydroxide as novel filler for high energy density dielectric polymer composites. *Compos Sci Technol* 172:117–124. <https://doi.org/10.1016/j.compscitech.2019.01.010>
 32. Dhatarwal P, Sengwa RJ (2020) Structural and dielectric characterization of (PVP/PEO)/Al₂O₃ nanocomposites for biodegradable nanodielectric applications. *Adv Composites Hybrid Mater* 3(3):344–353. <https://doi.org/10.1007/s42114-020-00168-y>
 33. Guo Y, Meng N, Xu J, Zhang K, Zhang Q, Pawlikowska E et al (2019) Microstructure and dielectric properties of Ba_{0.6}Sr_{0.4}TiO₃/(acrylonitrile-butadiene-styrene)-poly(vinylidene fluoride) composites. *Adv Composites Hybrid Mater* 2(4):681–619. <https://doi.org/10.1007/s42114-019-00114-7>
 34. Mao F, Shi Z, Wang J, Zhang C, Yang C, Huang M (2018) Improved dielectric permittivity and retained low loss in layer-structured films via controlling interfaces. *Adv Composites Hybrid Mater* 1(3):548–557. <https://doi.org/10.1007/s42114-018-0041-6>
 35. Sengwa RJ, Choudhary S, Dhatarwal P (2019) Investigation of alumina nanofiller impact on the structural and dielectric properties of PEO/PMMA blend matrix-based polymer nanocomposites. *Adv Composites Hybrid Mater* 2(1):162–175. <https://doi.org/10.1007/s42114-019-00078-8>
 36. Wang Q, Zhang J, Zhang Z, Hao Y, Bi K (2020) Enhanced dielectric properties and energy storage density of PVDF nanocomposites by co-loading of BaTiO₃ and CoFe₂O₄ nanoparticles. *Adv Composites Hybrid Mater* 3(1):58–65. <https://doi.org/10.1007/s42114-020-00138-4>
 37. Zhang G, Brannum D, Dong D, Tang L, Allahyarov E, Tang S et al (2016) Interfacial polarization-induced loss mechanisms in polypropylene/BaTiO₃ nanocomposite dielectrics. *Chem Mater* 28(13):4646–4660. <https://doi.org/10.1021/acs.chemmater.6b01383>
 38. Chen H, Pan Z, Wang W, Chen Y, Xing S, Cheng Y et al (2021) Ultrahigh discharge efficiency and improved energy density in polymer-based nanocomposite for high-temperature capacitors application. *Compos A Appl Sci Manuf* 142. <https://doi.org/10.1021/10.1016/j.compositesa.2020.106266>
 39. Zhu Y, Zhu Y, Huang X, Chen J, Li Q, He J et al (2019) High energy density polymer dielectrics interlayered by assembled boron nitride nanosheets. *Adv Energy Mater* 9(36). <https://doi.org/10.1002/aenm.201903062>
 40. Shen ZH, Wang JJ, Jiang JY, Huang SX, Lin YH, Nan CW et al (2019) Phase-field modeling and machine learning of electric-thermal-mechanical breakdown of polymer-based dielectrics. *Nat Commun* 10(1):1843. <https://doi.org/10.1038/s41467-019-09874-8>
 41. Shen ZH, Wang JJ, Lin Y, Nan CW, Chen LQ, Shen Y (2018) High-throughput phase-field design of high-energy-density polymer nanocomposites. *Adv Mater* 30(2). <https://doi.org/10.1002/adma.201704380>
 42. Guo YQ, Wang SS, Ruan KP, Zhang HT, Gu JW (2021) Highly thermally conductive carbon nanotubes pillared exfoliated graphite/polyimide composites. *npj Flex Electron* 5:16. <https://doi.org/10.1038/s41528-021-00113-z>
 43. Ruan KP, Guo YQ, Gu JW (2021) Liquid crystalline polyimide films with high intrinsic thermal conductivities and robust toughness. *Macromolecules* 54(10):4934–4944. <https://doi.org/10.1021/acs.macromol.1c00686>
 44. Chi Q, Gao Z, Zhang T, Zhang C, Zhang Y, Chen Q et al (2018) Excellent energy storage properties with high-temperature stability in sandwich-structured polyimide-based composite films. *ACS Sustain Chem Eng* 7(1):748–757. <https://doi.org/10.1021/acssuschemeng.8b04370>
 45. Sun W, Lu X, Jiang J, Zhang X, Hu P, Li M et al (2017) Dielectric and energy storage performances of polyimide/BaTiO₃ nanocomposites at elevated temperatures. *J Appl Phys* 121(24). <https://doi.org/10.1063/1.4989973>
 46. Liu J, Li X, Ma S, Zhang J, Jiang Z, Zhang Y (2020) Enhanced high-temperature dielectric properties of poly(aryl ether sulfone)/BaTiO₃ nanocomposites via constructing chemical crosslinked networks. *Macromol Rapid Commun* 41(24). <https://doi.org/10.1002/marc.202000012>
 47. Liu J, Shen Z, Xu W, Zhang Y, Qian X, Jiang Z et al (2020) Interface-strengthened polymer nanocomposites with reduced

- dielectric relaxation exhibit high energy density at elevated temperatures utilizing a facile dual crosslinked network. *Small* 16(22). <https://doi.org/10.1002/sml.202000714>
48. Li Q, Liu F, Yang T, Gadinski MR, Zhang G, Chen LQ et al (2016) Sandwich-structured polymer nanocomposites with high energy density and great charge-discharge efficiency at elevated temperatures. *Proc Natl Acad Sci U S A* 113(36):9995–10000. <https://doi.org/10.1073/pnas.1603792113>
 49. Hu P, Sun W, Fan M, Qian J, Jiang J, Dan Z et al (2018) Large energy density at high-temperature and excellent thermal stability in polyimide nanocomposite contained with small loading of BaTiO₃ nanofibers. *Appl Surf Sci* 458:743–750. <https://doi.org/10.1016/j.apsusc.2018.07.128>
 50. Li H, Ai D, Ren L, Yao B, Han Z, Shen Z et al (2019) Scalable polymer nanocomposites with record high-temperature capacitive performance enabled by rationally designed nanostructured inorganic fillers. *Adv Mater* 31(23). <https://doi.org/10.1002/adma.201900875>
 51. Zhang Q, Chen X, Zhang B, Zhang T, Lu W, Chen Z et al (2021) High-temperature polymers with record-high breakdown strength enabled by rationally designed chain-packing behavior in blends. *Matter*. <https://doi.org/10.1016/j.matt.2021.04.026>
 52. Dong J, Hu R, Xu X, Chen J, Niu Y, Wang F et al (2021) A facile in situ surface-functionalization approach to scalable laminated high-temperature polymer dielectrics with ultrahigh capacitive performance. *Adv Func Mater*. <https://doi.org/10.1002/adfm.202102644>

Publisher's Note Springer Nature remains neutral with regard to jurisdictional claims in published maps and institutional affiliations.